Formation dynamics of an entangled photon pair: A temperature-dependent analysis

Alexander Carmele,[1,*] Frank Milde,[1] Matthias-René Dachner,[1] Malek Bagheri Harouni,[2] Rasoul Roknizadeh,[2,3] Marten Richter,[1] and Andreas Knorr[1]

[1]*Institut für Theoretische Physik, Nichtlineare Optik und Quantenelektronik, Technische Universität Berlin, Hardenbergstraße 36, EW 7-1 10623 Berlin, Germany*

[2]*Physics Department, Quantum Optics Group, University of Isfahan, 81746 Isfahan, Iran*

[3]*Laser-Plasma Research Institute, Shahid Beheshti University, G. C., Evin, 19839-63113 Tehran, Iran*

(Received 28 October 2009; revised manuscript received 22 April 2010; published 26 May 2010)

We theoretically study the polarization entanglement of photons generated by the biexciton cascade in a GaAs/InAs semiconductor quantum dot (QD) located in a nanocavity. A detailed analysis of the complex interplay between photon and carrier coherences and phonons which occurs during the cascade allows us to clearly identify the conditions under which entanglement is generated and destroyed. A quantum state tomography is evaluated for varying exciton fine-structure splittings. Also, by constructing an effective multiphonon Hamiltonian which couples the continuum of the QD-embedding wetting layer states to the quantum confined states, we investigate the relaxation of the biexciton and exciton states. This consistently introduces a temperature dependence to the cascade. Considering typical Stranski-Krastanov grown QDs for temperatures around 80 K the degree of entanglement starts to be affected by the dephasing of the exciton states and is ultimately lost above 100 K.

DOI: 10.1103/PhysRevB.81.195319 PACS number(s): 78.67.Hc, 42.50.Dv, 63.22.−m, 71.35.−y

I. INTRODUCTION

In recent years, photons as qubits have been sent successfully over fiber communication channels,[1,2] quantum cryptography is technically feasible[3,4] and quantum teleportation of so-called entangled photon states was demonstrated.[5,6] Entanglement in its simplest form is a nonseparable superposition of joint quantum states, in our case qubits, that shows nonlocal quantum correlation. Among different proposals,[7–11] very promising solid-state sources for entangled photon pairs are semiconductor quantum dots (QDs).[12,13]

The prospect of all-integrated photonic applications in combination with compact semiconductor devices raises the question of how robust and efficient an embedded entangled photon source is when subjected to losses and dephasing due to naturally occurring interaction with its surrounding host material.

In this respect, Axt *et al.* investigated within a generating functions approach in Ref. 14 the dephasing of an exciton-biexciton QD system, which is coupled to an arbitrary number of phonon modes. With the focus on photon entanglement, Hohenester *et al.* considered in Ref. 15 the elastic phonon scattering at the device boundaries on a master equation level.

In this paper, we present microscopic calculations of a phonon-assisted biexciton cascade in an InAs QD embedded in an InGaAs wetting layer (WL).[16] The coupling of the discrete QD states to the WL continuum via multiphonon processes[17] leads to dephasing rates that significantly limit the entanglement output efficiency for high temperatures (above 100 K). An equation of motion approach allows us to perform a quantum-state tomography of the photon density matrix and to calculate the concurrence of the polarization-entangled photons for experimentally accessible external parameters such as temperature, exchange splitting, or WL carrier density.

The paper is organized as follows. After the considered system and calculated observables are introduced in more detail in Sec. II, the different interactions of the QD carriers with phonons and cavity photons are discussed in Sec. III. Then the coupled equations of motion are derived, their dynamics evaluated, and the results presented in Secs. IV A and IV B.

II. CHARACTERIZATION, GENERATION, AND MEASUREMENT OF ENTANGLED PHOTONS

A. Fine structure of quantum dots and generation of entangled photons

The atomlike discrete energy levels of a QD can be pumped electrically[18,19] or by photoexcitation,[20] where electrons in the WL conduction band (c) and holes in the WL valence band (v) are created. The carriers subsequently relax into the QD and occupy the discrete energy shells.[21] In the strong confinement regime, the relevant single-particle basis is constructed by the heavy hole (HH) with total angular momentum $J_h=3/2$ and spin projection in growth direction $m_{j,h}=\pm 3/2$ and the electron with $J_e=1/2$, $m_{j,e}=\pm 1/2$, as shown in Fig. 1(a).[22,23]

When the carriers occupy the lowest shell, two excitons can form a bound singlet state, a biexciton ($|B\rangle$).[23] Under emission of a σ_+ or σ_- polarized first so-called biexciton photon, the system enters into an intermediate, optically allowed exciton state. In a D_{2d}-symmetric QD, these bright exciton states, denoted by $|X_\pm\rangle$, are degenerate and couple to $\sigma_\pm$ circularly polarized light [σ_+ (σ_-) labels right-handed (left-handed) circularly polarized light], as depicted in Fig. 1(b).[24,25] Subsequently, the QD carriers relax into the ground state ($|G\rangle$) by emitting a second so-called exciton photon. As a consequence of total angular-momentum conservation, both emitted photons are of opposite circular polarization,[26]

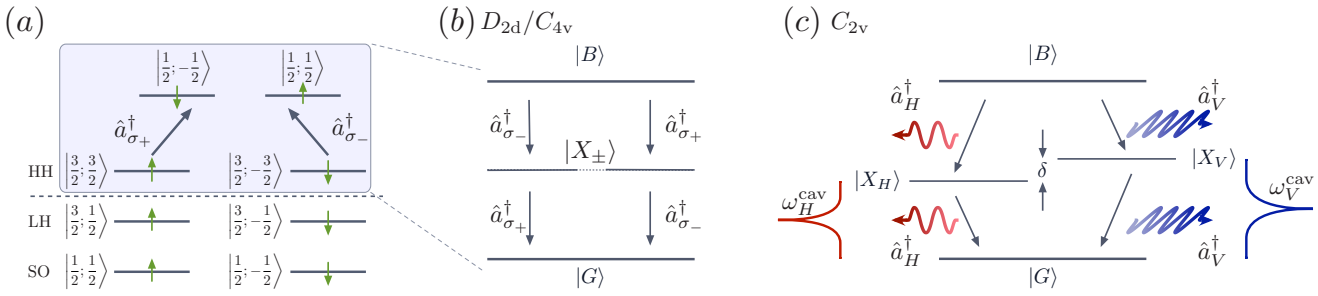

FIG. 1. (Color online) (a) QD band structure with spin states $s=|J;m_j\rangle$. Since the light hole (LH) and split-off (SO) states lie energetically well below the heavy hole (HH) states, only the latter and the electron states are relevant for the biexcitonic framework. (b) Cascade of a symmetric QD with degenerate exciton states $|X_\pm\rangle$. (c) Cascade with a FSS $\delta\neq 0$ (without biexcitonic shift). There are two possible paths: either two photons with vertical V or horizontal H polarization are emitted into a cavity mode $\omega_{V/H}^{cav}$ with a spectral FWHM κ. For vanishing FSS, δ the which-path information is lost and the photons are polarization entangled. With a FSS $\delta\neq 0$, the photons are not fully polarization entangled.

see Fig. 1(b). Since the exciton states $|X_\pm\rangle$ are degenerate, i.e., no fine-structure splitting (FSS) δ is present, their decay path can only be determined by their polarization, otherwise they are indistinguishable.[27]

With an asymmetry in the semiconductor crystal, the nonclassical correlation of the photons is often spoiled. Under strain, the dot's symmetry reduces to C_{2v} and the anisotropic electron-hole exchange interaction splits the exciton doublet into two states, $|X_H\rangle=1/\sqrt{2}(|X_+\rangle+|X_-\rangle)$ and $|X_V\rangle=1/\sqrt{2}(|X_+\rangle-|X_-\rangle)$, energetically separated by the FSS δ, shown in Fig. 1(c). These states couple to photon modes of orthogonal linear polarization along the direction of one crystallographic axis, labeled horizontal (H) and vertical (V), respectively. The energetic separation of these states superimposes a which-path information onto the emitted photon frequencies and the degree of their entanglement is reduced. In typical experiments, to efficiently collect the photons, the QD is placed inside a cavity supporting only two modes of different polarizations V and H with frequencies $\omega_V^{cav}\neq\omega_H^{cav}$.[28] Here, these modes are assumed to be in resonance with the corresponding exciton-ground-state transitions with a full width at half maximum (FWHM) of $\kappa=10$ μeV. Due to the finite line width of the cavity modes, the slightly detuned biexciton-exciton transition can still emit into the same corresponding modes $\omega_{V/H}^{cav}$, see Fig. 1(c).

Although the ideal case of zero splitting can be recovered,[13,29] phonons as a decoherence mechanisms will have an impact on the performance of a QD as a source of polarization-entangled photons, in particular, at elevated temperatures. To provide a meaningful quantitative measure of the entanglement, the next section will introduce the concurrence.

B. Measure of entanglement—relevant quantities

Quantum-state tomography[30] provides a measurement scheme which gives access to the different elements of the photon density matrix ρ^{pt}. They are experimentally reconstructed by measuring the two-photon cross-correlation function $g_{ij}^2(t,\tau)$ (Ref. 31) over a mean photon-arrival time t. The function $g_{ij}^2(t,\tau)$ corresponds to the polarization correlation between a biexciton photon emitted at time t and the subsequent exciton photon at time $t+\tau$ (Ref. 32)

$$g_{ij}^2(t,\tau)\propto\langle a_i^\dagger(t)a_i^\dagger(t+\tau)a_j(t+\tau)a_j(t)\rangle. \tag{1}$$

The correlation function is written in terms of photon creation ($a_i^\dagger$) and annihilation (a_j) operators of the different photon modes $i,j\in\{H,V\}$, cf. Fig. 1(c).

Since on average the two emitted photons exhibit a delay time τ, we consider an experimental Hanbury Brown and Twist-type setup, where the distance within the two light paths to the detector is appropriately adjusted to compensate τ.[29,33] This will enhance the probability to detect the two photons at the same time. To present an easy accessible analysis of the photon cascade we consider of all the statistically distributed photon emissions solely such events were the compensated delay time indeed is zero. In time-integrated measurements, the temporal dynamics of the density-matrix element $\langle ii|\rho^{pt}|jj\rangle$ is time averaged over the arrival times t (Refs. 30 and 32)

$$\rho_{ij}:=\langle ii|\rho^{pt}|jj\rangle=\frac{1}{T}\int_0^T g_{ij}^2(t',0)dt'. \tag{2}$$

Thus, the source of entanglement can be characterized by $\rho_{HV}\propto\langle\hat{a}_V^\dagger\hat{a}_V^\dagger\hat{a}_H\hat{a}_H\rangle$. The usual expression for the degree of entanglement is the concurrence C (Refs. 34 and 35)

$$C=2|\rho_{HV}|. \tag{3}$$

III. MODELING AN EMBEDDED QUANTUM DOT AS A SEMICONDUCTOR SOURCE OF ENTANGLEMENT

A. Hamiltonian and QD model

The coupled dynamics of observables, including the photon correlation function g_{ij}^2, cf. Eq. (1), can be generally derived from the system's Hamilton operator $\hat{H}$ via Heisenberg's equation of motion

$$-i\hbar\partial_t\langle\hat{O}\rangle=\langle[\hat{H},\hat{O}]_-\rangle. \tag{4}$$

A general setup of a two-level QD (Ref. 13) coupled to the WL continuum inside a nanocavity is displayed in Fig. 2 and its Hamiltonian is given by

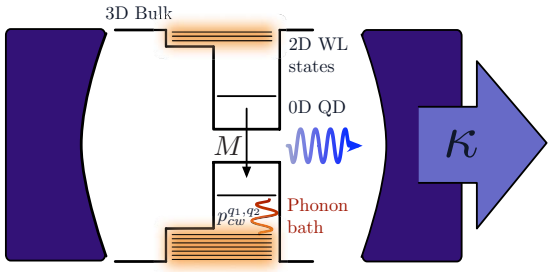

FIG. 2. (Color online) General system scheme. Two electron-hole pairs in a QD are coupled to the continuum of WL states via an effective LO phonon interaction $p_{cw}^{q_1,q_2}$. The phonons are treated as a thermal bath. The QD has two levels with a conduction and a valence band level and is placed inside a cavity. Here, the carriers interact with photons via the electron-light coupling element M, where a photon loss via κ is assumed.

$$\hat{H} = \hat{H}^{c}_{QD,0} + \hat{H}^{c}_{WL,0} + \hat{H}^{pt}_{0} + \hat{H}^{pn}_{0} + \hat{H}^{c\text{-}c}_{QD} + \hat{H}^{c\text{-}pt}_{QD} + \hat{H}^{c\text{-}pn}_{QD,WL} + \hat{H}^{c\text{-}pn}_{WL,WL}. \quad (5)$$

First, the kinetic energy of the confined QD carriers $\hat{H}^{c}_{QD,0}=\Sigma_s(\varepsilon_v^{QD}\hat{h}_s^\dagger\hat{h}_s+\varepsilon_c^{QD}\hat{e}_s^\dagger\hat{e}_s)$ and the WL carriers $\hat{H}^{c}_{WL,0}=\Sigma_{\mathbf{k}s}\varepsilon_{v\mathbf{k}}^{WL}\hat{w}_{\mathbf{k}s}^\dagger\hat{w}_{\mathbf{k}s}$ appears. Fermionic operators describe electrons and holes, where heavy holes in the v band (operator $\hat{h}_s$) and electrons in the c band (operator $\hat{e}_s$) are included. Here, the carrier spin state $s=|J,m_j\rangle$ is given for the holes (electrons) by $\uparrow=|3/2;3/2\rangle$ ($\uparrow=|1/2;1/2\rangle$) and $\downarrow=|3/2;-3/2\rangle$ ($\downarrow=|1/2;-1/2\rangle$). Similar to the operators for the confined states, $\hat{w}_{\mathbf{k}s}^\dagger$ ($\hat{w}_{\mathbf{k}s}$) are creators (annihilators) of a hole carrier in the WL continuum of the v band with spin state s and wave vector $\mathbf{k}$. For the WL carriers, we take into account only the hole contributions of the v band, motivated in the next section. The impact of spin-orbit coupling on the carrier's energy can be neglected in QDs,[36] and thus ε_i is assumed to be independent of the carrier's spin state.

The energy of the cavity photons and of the semiconductor bulk phonons is described by $\hat{H}^{pt}_{0}=\Sigma_i\hbar\omega_i\hat{a}_i^\dagger\hat{a}_i$ and $\hat{H}^{pn}_{0}=\Sigma_{\mathbf{q}}\hbar\omega_{LO}\hat{b}_{\mathbf{q}}^\dagger\hat{b}_{\mathbf{q}}$. The Bosonic longitudinal optical (LO) phonon creation (annihilation) operators at wave vector $\mathbf{q}$ are denoted by $\hat{b}_{\mathbf{q}}^\dagger$ ($\hat{b}_{\mathbf{q}}$). The dispersion of the optical phonon is treated within the Einstein approximation with $\hbar\omega_{LO}=36.4$ meV.

The carrier-carrier interaction is included via $\hat{H}^{c\text{-}c}_{QD}$.[14] The electron-hole pairs in the QD interact with the cavity photons of the quantized light field via $\hat{H}^{c\text{-}pt}_{QD}$. For a more detailed derivation of $\hat{H}^{c\text{-}pt}_{QD}$ and $\hat{H}^{c\text{-}c}_{QD}$, see Appendices A and B.

The interaction of the WL with the QD states via LO phonons is considered in $\hat{H}^{c\text{-}pn}_{QD,WL}$ and the electron-phonon coupling within the WL in $\hat{H}^{c\text{-}pn}_{WL,WL}$. Both are discussed in more detail in the next section, as they lead to temperature-dependent dephasing rates (see Sec. III B).

B. Multiphonon coupling of WL and QD

Embedded in a host material, quantum-confined electrons in Stranski-Krastanov grown InAs/GaAs QDs interact via LO phonons with a continuum of two-dimensional (2D) electronic WL states only a few tens millielectron volt away.[21] This typically leads to temperature-dependent dephasing times for the QD states.[37–40] In the model regarded here, we restrict our investigation on the contributions of LO phonons.[41,42]

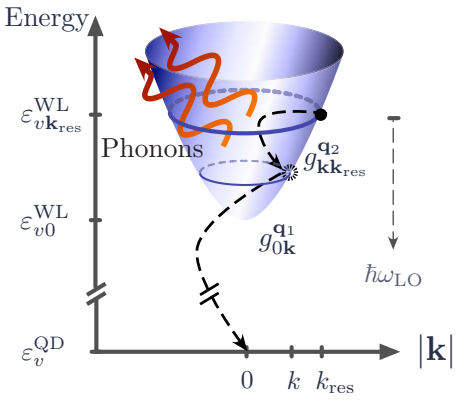

FIG. 3. (Color online) Wetting layer system scheme. Shown in blue is the parabolic 2D dispersion of the WL holes $\hbar^2\mathbf{k}^2/(2m_h^*)$. Marked on the energy scale are (i) the WL band edge ε_{v0}^{WL} which is energetically separated from the QD v shell ε_v^{QD} by more than a single-phonon energy: $\Delta\varepsilon_v^{QD}=\varepsilon_{v0}^{WL}-\varepsilon_v^{QD}>\hbar\omega_{LO}$, (ii) the WL states at $\mathbf{k}_{res}$ resonant with a two-phonon transition $\varepsilon_{v\mathbf{k}_{res}}^{WL}=\varepsilon_v^{QD}+2\hbar\omega_{LO}$ to the QD. The transition from the resonant states to the QD pass through intermediate states at $\varepsilon_{v\mathbf{k}}^{WL}$ with probability amplitude $g_{\mathbf{k}_2\mathbf{k}_1}^{\mathbf{q}}$.

Depending on the dot size,[21] the QD HH state is typically separated more than one, but less than two LO phonon energies $\hbar\omega_{LO}$ from the WL band edge, see Fig. 3. Therefore, to effectively connect the QD holes with the WL, at least two-phonon processes have to be taken into account, whereas single-phonon processes do not contribute. Within the two-phonon limit, the influence of the WL conduction band on the QD electrons can be neglected, because, typically, more than two LO phonons are necessary to bridge the energy gap to the QD state. Therefore, the dephasing is dominantly determined by the hole-WL interaction only. Moreover, the mutual Coulomb interaction of the WL carriers is not included as the carrier densities considered here are low.[40] Under these assumptions, microscopic dephasing rates can be derived by using an effective Hamiltonian approach which originates from a multiphoton theory.[43] From the Hamiltonian in Eq. (5) the following contributions are used to calculate the LO-phonon-induced dephasing:

$$\hat{H}_{QD,WL} = \hat{H}^{c}_{QD,0} + \hat{H}^{c}_{WL,0} + \hat{H}^{pn}_{0} + \hat{H}^{c\text{-}pn}_{QD,WL} + \hat{H}^{c\text{-}pn}_{WL,WL}.$$

Here, the phonon-mediated interaction between QD holes and WL states and the carrier-phonon interaction within the WL are given by

$$\hat{H}^{c\text{-}pn}_{QD,WL} = \sum_s \sum_{\mathbf{kq}} g_{0\mathbf{k}}^{\mathbf{q}}\hat{h}_s^\dagger\hat{w}_{\mathbf{k}s}(\hat{b}_{\mathbf{q}} + \hat{b}_{-\mathbf{q}}^\dagger) + \text{H.a.},$$

$$\hat{H}^{\text{c-pn}}_{\text{WL,WL}} = \sum_{s} \sum_{\mathbf{k}\mathbf{k}'\mathbf{q}} g^{\mathbf{q}}_{\mathbf{k}\mathbf{k}'} \hat{w}^{\dagger}_{\mathbf{k}s} \hat{w}_{\mathbf{k}'s} (\hat{b}_{\mathbf{q}} + \hat{b}^{\dagger}_{-\mathbf{q}}) + \text{H.a.},$$

where H.a. stands for hermitian adjoint. The Fröhlich coupling elements are $g^{\mathbf{q}}_{\mathbf{k}\mathbf{k}'}$, which can be found in Ref. 44. Within a projection-operator-based theory,[43] $\hat{H}_{\text{QD,WL}}$ is mapped onto the resonant WL states and becomes

$$\hat{H}_{\text{QD,WL}} = \hat{H}^{\text{c}}_{\text{QD},0} + \hat{H}^{\text{c}}_{\text{WL},0} + \hat{H}_{\text{eff}} \tag{6}$$

with the effective LO-phonon-assisted WL influence on the QD holes in $\hat{H}_{\text{eff}}$. All other off-resonant contributions are implicitly included in the coupling elements of the effective Hamiltonian. Taking only two-phonon processes into account, $\hat{H}_{\text{eff}}$ reads[45]

$$\hat{H}_{\text{eff}} = \sum_{s} \sum_{\mathbf{q}_1\mathbf{q}_2\mathbf{k}_{\text{res}}} p^{\mathbf{q}_1\mathbf{q}_2}_{cw,s} \hat{h}^{\dagger}_{s} \hat{w}_{\mathbf{k}_{\text{res}}s} \hat{b}_{\mathbf{q}_1} \hat{b}_{\mathbf{q}_2} + \sum_{s} \sum_{\mathbf{q}_1\mathbf{q}_2\mathbf{k}_{\text{res}}} p^{\mathbf{q}_1\mathbf{q}_2}_{wc,s} \hat{w}^{\dagger}_{\mathbf{k}_{\text{res}}s} \hat{h}_{s} \hat{b}^{\dagger}_{\mathbf{q}_1} \hat{b}^{\dagger}_{\mathbf{q}_2}, \tag{7}$$

with the effective coupling elements

$$p^{\mathbf{q}_1\mathbf{q}_2}_{cw,s} = \sum_{\substack{\mathbf{k} \\ \mathbf{k}\neq\mathbf{k}_{\text{res}}}} \frac{g^{\mathbf{q}_1}_{0\mathbf{k}} g^{\mathbf{q}_2}_{\mathbf{k}\mathbf{k}_{\text{res}}} (1 - \langle \hat{w}^{\dagger}_{\mathbf{k}s} \hat{w}_{\mathbf{k}s} \rangle)}{\varepsilon^{\text{WL}}_{v\mathbf{k}} - \varepsilon^{\text{QD}}_{v} - \hbar\omega_{\text{LO}}}. \tag{8}$$

The coupling elements contain Pauli-blocking terms $(1 - \langle \hat{w}^{\dagger}_{\mathbf{k}s} \hat{w}_{\mathbf{k}s} \rangle)$ and therefore depend on the temperature and the WL carrier occupation.[19,46] The WL holes $\hat{w}^{(\dagger)}_{\mathbf{k}_{\text{res}}s}$ in $\hat{H}_{\text{eff}}$ have an energy of exactly two-phonon energies from the QD state energy. A transition from these resonant WL holes at $\varepsilon^{\text{WL}}_{v\mathbf{k}_{\text{res}}}$ to the QD shell takes place under simultaneous emission of two phonons. The whole process is energy conserving: $\varepsilon^{\text{WL}}_{v\mathbf{k}_{\text{res}}} - \varepsilon^{\text{QD}}_{v} = 2\hbar\omega_{\text{LO}}$. In contrast, in the transition to the intermediate state at $\varepsilon^{\text{WL}}_{v\mathbf{k}}$, energy conservation is always violated, since the hole state at $\mathbf{k}$ is separated less than $\hbar\omega_{\text{LO}}$ from $\varepsilon^{\text{WL}}_{v\mathbf{k}_{\text{res}}}$ but more than $\hbar\omega_{\text{LO}}$ from the QD state, see Fig. 3. This means that within the time-energy uncertainty, carriers relax in a higher-order Markovian process and can violate the energy conservation in the intermediate steps.

The probability amplitude for these intermediate transitions are $g^{\mathbf{q}_2}_{\mathbf{k}\mathbf{k}_{\text{res}}}$ and $g^{\mathbf{q}_1}_{0\mathbf{k}}$. Equation (8) shows that all possible transitions between the QD and the WL are mediated by all off-resonant WL states $\mathbf{k}$. The strength of the coupling element is determined by to what extent the energy-conservation condition in the denominator is met in every phonon-assisted electronic transition. We can use the effective Hamiltonian (6) to derive relaxation and dephasing rates using Heisenberg equations of motion, where the hierarchy problem is treated within a Born factorization.[45,47,48] The calculations lead to the following equations for the QD states:

$$\frac{d}{dt}\langle \hat{e}^{\dagger}_{s} \hat{h}^{\dagger}_{s} \rangle = -(i\hbar\Omega_0 + \Gamma_{w,s}) \langle \hat{e}^{\dagger}_{s} \hat{h}^{\dagger}_{s} \rangle, \tag{9}$$

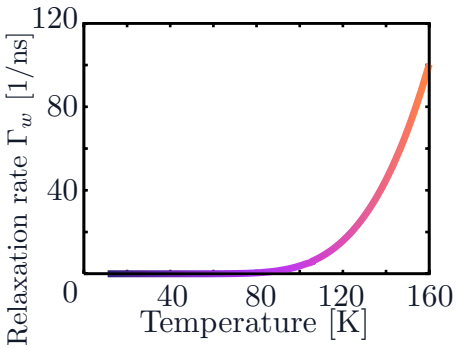

FIG. 4. (Color online) The phonon-induced relaxation rate Γ_w as a function of temperature T. At about 80 K, Γ_w has approached 1 ns^{-1} and starts to contribute strongly to the decay of the QD states.

$$\frac{d}{dt}\langle \hat{h}^{\dagger}_{s} \hat{h}_{s} \rangle = -2\Gamma_{w,s} \langle \hat{h}^{\dagger}_{s} \hat{h}_{s} \rangle \tag{10}$$

with the QD gap energy $\hbar\Omega_0 = \varepsilon^{\text{QD}}_{c} - \varepsilon^{\text{QD}}_{v}$ and the WL-induced damping rate[45]

$$\Gamma_{w,s} = [(1 - f_{h,s})(n+1)^2 + f_{h,s} n^2] \gamma_s. \tag{11}$$

The damping γ_s is given by

$$\gamma_s = \int\int d^3q_1 d^3q_2 p^{\mathbf{q}_1\mathbf{q}_2}_{cw,s} (p^{\mathbf{q}_1\mathbf{q}_2}_{wc,s} + p^{\mathbf{q}_2\mathbf{q}_1}_{wc,s}). \tag{12}$$

In Eq. (11), $f_{h,s} = \Sigma_{\mathbf{k}_{\text{res}}} \langle \hat{w}^{\dagger}_{\mathbf{k}_{\text{res}}s} \hat{w}_{\mathbf{k}_{\text{res}}s} \rangle$ is used for the WL hole density at the resonant energy, which in the carrier low-density limit is assumed to be zero. Note that this implies $\Gamma_w = \Gamma_{w,\uparrow} = \Gamma_{w,\downarrow}$. The phonon bath is characterized by the Bose-Einstein distribution $n = \langle \hat{b}^{\dagger} \hat{b} \rangle$. Figure 4 displays the temperature dependence of Γ_w.

The damping rates in Eqs. (9) and (10) consistently account for the relaxation of the QD electrons.[48] To discuss the polarization entanglement between two emitted photons, we proceed and determine the equations of motion governing the relevant observables' dynamics.

IV. RESULTS

A. Dynamics of the biexciton cascade

The overall dynamics aiming at the concurrence C is calculated within a density-matrix approach. The complete density operator ρ considers the electron-cavity photon system ρ^{s} and reservoirs ρ^{r} (LO phonons, WL carriers, and dissipative photon modes). Initially at time t_0, ρ factorizes $\rho(t_0) = \rho^{\text{s}}(t_0) \otimes \rho^{\text{r}}(t_0)$. The losses, in particular, the temperature-dependent WL-induced damping rates, cf. Eq. (11), are included via the reduced density matrix[49]

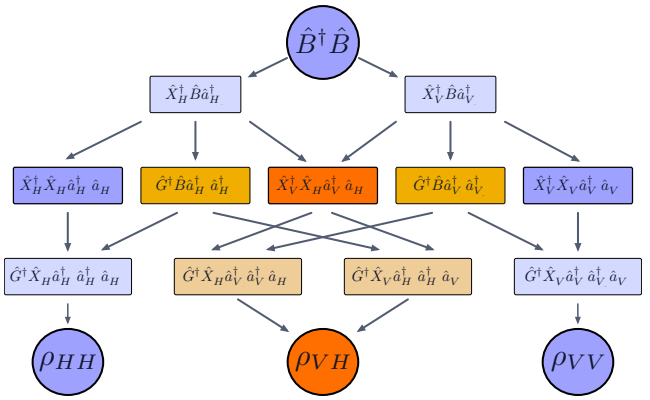

FIG. 5. (Color online) Equations of motion truncated to the pure cascade scheme. The dark blue quantities represent densities which do not contribute to entanglement, whereas the dark orange and red quantities directly generate a crossing of the different paths in the light orange boxes and are crucial to entanglement.

$$\partial_t\rho^{\mathrm{s}}(t) = -\frac{i}{\hbar}\mathrm{Tr}_{\mathrm{r}}[V(t),\rho^{\mathrm{s}}(t_0)\otimes\rho^{\mathrm{r}}(t_0)] - \frac{1}{\hbar^2}\mathrm{Tr}_{\mathrm{r}}\int_{t_0}^{t}\{V(t),[V(t'),\rho^{\mathrm{s}}(t)\otimes\rho^{\mathrm{r}}(t_0)]\}dt'. \tag{13}$$

The interaction with the reservoirs appears in V [e.g., $\hat{H}_{\mathrm{eff}}$, see Eq. (7)]. In a Markov approximation, this leads to a decay of the QD populations and dephasing contributions to the QD transitions due to their environment coupling.[48] The calculated damping rates Γ_w from Eqs. (9) and (10) correspond to a T_1 time and are incorporated like the radiative dephasing Γ_{rad} in the Weisskopf-Wigner theory.[31,49–51] Both occur and lead to an overall damping of $\Gamma=\Gamma_{\mathrm{rad}}+\Gamma_w$. The electron-cavity photon dynamics is calculated via the Liouville-von Neumann equation:[52] $i\hbar\partial_t\rho^{\mathrm{s}}=[\hat{H},\rho^{\mathrm{s}}]$, with the total excitonic Hamiltonian

$$\hat{H} = \sum_{i=H,V}\hbar\omega_i^{\mathrm{cav}}\hat{a}_i^\dagger\hat{a}_i + \hbar\omega_G\hat{G}^\dagger\hat{G} + \hbar\omega_H\hat{X}_H^\dagger\hat{X}_H + \hbar\omega_V\hat{X}_V^\dagger\hat{X}_V + \hbar\omega_B\hat{B}^\dagger\hat{B} + \hbar M(\hat{G}^\dagger\hat{X}_H\hat{a}_H^\dagger + \hat{G}^\dagger\hat{X}_V\hat{a}_V^\dagger + \hat{X}_H^\dagger\hat{B}\hat{a}_H^\dagger - \hat{X}_V^\dagger\hat{B}\hat{a}_V^\dagger + \mathrm{H.a.}).$$

For an arbitrary operator $\hat{O}$, one can derive the temporal evolution of the expectation value $\langle O\rangle$ by

$$\mathrm{Tr}(\partial_t\rho^{\mathrm{s}}\hat{O}) = \partial_t\langle\hat{O}\rangle = -\frac{i}{\hbar}\mathrm{Tr}([\hat{H},\rho^{\mathrm{s}}]\hat{O}) = \frac{i}{\hbar}\langle[\hat{H},\hat{O}]\rangle.$$

An overview of the complex dynamics of the considered correlation functions is given in Fig. 5, which unravels the consequential interplay of the different quantities step by step. A given biexciton density (initial condition) can decay via two possible paths (left H and right V) and finally generate a photon pair ρ_{ij} $(i,j\in\{H,V\}$, cf. bottom of Fig. 5). In a first step, a photon-assisted coherence $\hat{X}_i^\dagger\hat{B}\hat{a}_i^\dagger$ (light blue box) builds up, which then contributes to (i) a cross-polarization coherence $\hat{X}_V^\dagger\hat{X}_H\hat{a}_V^\dagger\hat{a}_H$ (red box), particularly important to achieve entanglement in ρ_{VH}, (ii) a two-photon coherence $\hat{G}^\dagger\hat{B}\hat{a}_i^\dagger\hat{a}_i^\dagger$ (light orange box), which also leads to an interference of the two paths and thus contributes to ρ_{VH}, or (iii) a combined exciton-photon density $\hat{X}_i^\dagger\hat{X}_i\hat{a}_i^\dagger\hat{a}_i$ (dark blue box), which does not influence the degree of entanglement. This gives meaningful insight into the underlying formation process of polarization entanglement. In the weak-coupling regime, only spontaneous emission in the cascade is taken into account.

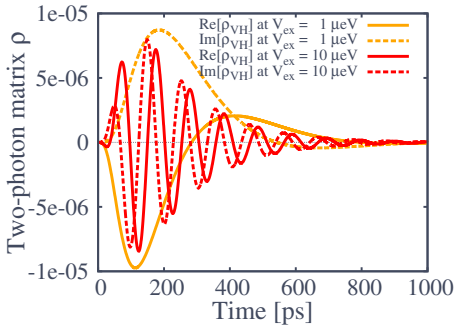

FIG. 6. (Color online) Temporal evolution of the nonintegrated off-diagonal two-photon density-matrix elements at $T=0$ K [real (solid) and imaginary (dashed) parts] for $V_{\mathrm{ex}}=1$ μeV (orange) and $V_{\mathrm{ex}}=10$ μeV (red). With increasing V_{ex}, the oscillations become more rapid.

The concurrence C, as a measure for the degree of entanglement, is determined by the photon density matrix, cf. Eq. (3). It is given by the off-diagonal element ρ_{VH}

$$\partial_t\langle\hat{a}_V^\dagger\hat{a}_V^\dagger\hat{a}_H\hat{a}_H\rangle = 2i(\omega_V^{\mathrm{cav}}-\omega_H^{\mathrm{cav}}+2i\kappa)\langle\hat{a}_V^\dagger\hat{a}_V^\dagger\hat{a}_H\hat{a}_H\rangle + 2iM(\langle\hat{G}^\dagger\hat{X}_H\hat{a}_V^\dagger\hat{a}_V^\dagger\hat{a}_H\rangle - \langle\hat{X}_V^\dagger\hat{G}\hat{a}_V^\dagger\hat{a}_H\hat{a}_H\rangle). \tag{14}$$

Beside its damping due to cavity losses[52] chosen to be $\kappa=10$ μeV, the two-photon correlation ρ_{VH} is driven by two higher-order correlations, cf. Fig. 5. Both include an exciton-ground-state transition $\hat{G}^\dagger\hat{X}_i$ under emission of a photon $\hat{a}_j^\dagger$ of opposite polarization as the $|X_i\rangle$ state would allow, e.g., $\hat{G}^\dagger\hat{X}_H\hat{a}_V^\dagger$. The transition process takes place in the presence of a photon coherence $\hat{a}_V^\dagger\hat{a}_H$ generated by the previous biexciton-exciton decay, see light-orange boxes in Fig. 5. As these terms already include a single-photon coherence and generate a second one leading to a two-photon coherence, they are exactly the terms one would expect intuitively to contribute to ρ_{VH}. For a small FSS $\delta=2|V_{\mathrm{ex}}|=\omega_V^{\mathrm{cav}}-\omega_H^{\mathrm{cav}}$, the fixed cavity frequencies ω_V^{cav} and ω_H^{cav} are in close resonance, and ρ_{VH} will slowly oscillate on the time scale given by the corresponding FSS, see the orange curves (all at $T=0$ K) in Fig. 6. Here, the total set of equations of motion is numerically evaluated to obtain $\rho_{VH}(t)$ (detailed discussion in Sec. IV B). For an increasing FSS, on the other hand, both frequencies are detuned and ρ_{VH} shows a strong oscillating behavior, compare red curves in Fig. 6. Here, the temporal mean value of ρ_{VH} is close to zero, and thus no entanglement is observed in a time-averaged measurement, see Eq. (1), and

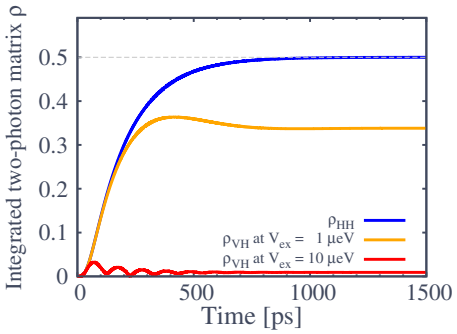

FIG. 7. (Color online) Averaged two-photon matrix elements at $T=0$ K. Their steady-state values give the quantum-state tomography.

the red curve (all at $T=0$ K) in Fig. 7 for the time-averaged ρ_{VH}. For large FSS this means that the two different decay paths are distinguishable, so that the photons are entirely emitted in either the H or the V cascade, and there is no overlap which is only generated by transitions like $\hat{G}^{\dagger}\hat{X}_H\hat{a}_V^{\dagger}$, containing both V and H indices. The which-path information is conserved. However, for small FSS, there is an uncertainty in the decay path and the photons become at least partially polarization entangled.

B. Quality of entanglement

In this section we discuss how temperature affects the concurrence and investigate the complete temporal dynamics of the cascade by numerically solving the whole set of equations of motion [Eq. (14)], Eqs. (C1)–(C14) given in Appendix C.

Since ρ^{pt} is experimentally reconstructed by photocounting experiments, all elements of ρ^{pt} are given by time integration.[32] Recalling and employing Eq. (2) to the results of Fig. 6, we discuss the time-averaged elements of ρ^{pt}. As can be seen in Fig. 7, the diagonal elements have a continuous positive slope and start to saturate around 0.5 ns. Here, the final value of the time-integrated diagonal elements is reached at about 1 ns.[53] However, the situation is very different for the off-diagonal elements, as they are complex quantities that oscillate when $V_{\mathrm{ex}} \neq 0$. Its absolute value (important for the concurrence) shows a nonmonotonous behavior in Fig. 7. Obviously, the experimentally measurable concurrence completely vanishes for a FSS higher than $V_{\mathrm{ex}}=20$ μeV.

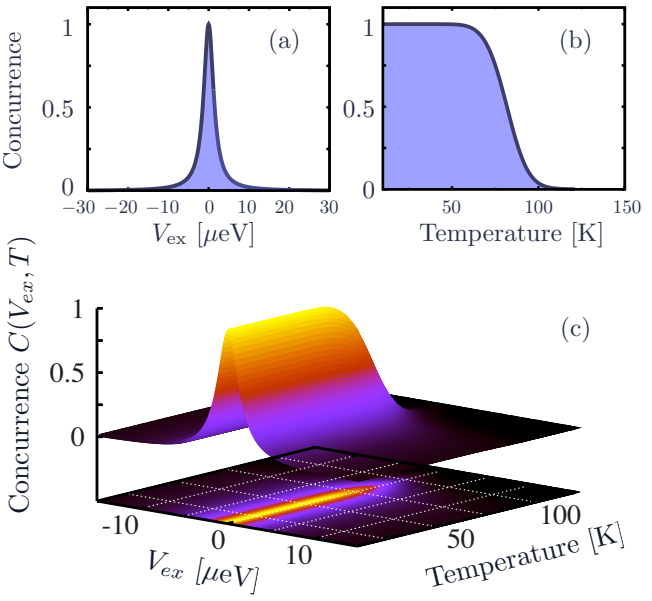

FIG. 9. (Color online) Plot of the concurrence. (a) displays C at 0 K as a function of V_{ex}. (b) illustrates the influence of the temperature due to the phonon-induced WL influence at $V_{\mathrm{ex}}=0$ μeV. Both temperature and V_{ex} dependences are shown in (c).

The concurrence will drop for increasing V_{ex} as the time-averaged ρ_{VH} does. This can be clearly seen in the quantum-state tomography shown in Fig. 8. The diagonal and the off-diagonal contributions are still in the same order of magnitude for $V_{\mathrm{ex}}=1$ μeV, cf. Fig. 8(a), but a loss can already be seen. For a larger splitting, ρ_{VH} vanishes in Fig. 8(b). Figure 9 constitutes the central result of this work—a temperature-dependent study of entanglement. First, Fig. 9(a) shows how the entanglement is lost with increasing FSS as a continuous function of V_{ex}. Here, the FWHM is determined by the values of the Coulomb parameters. When temperature effects of the WL states are taken into account, the concurrence can be spoiled even in the ideal situation of degenerate exciton states, see Fig. 9(b). For low tempera-

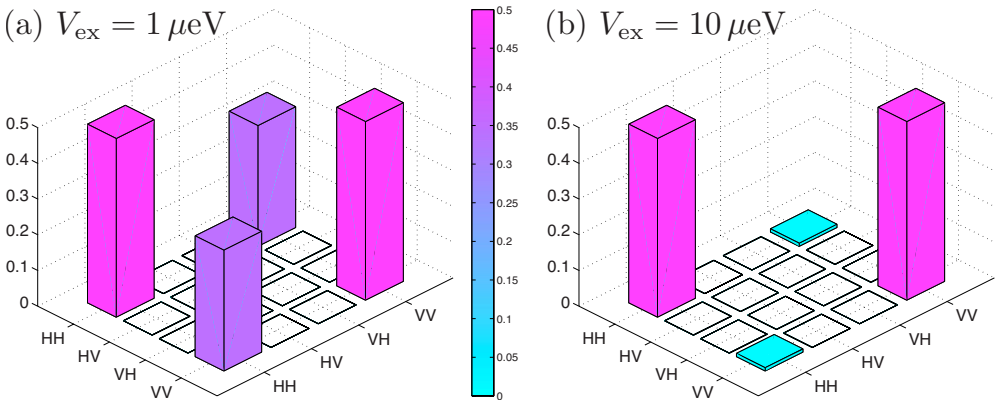

FIG. 8. (Color online) Quantum-state tomography for (a) $V_{\mathrm{ex}}=1$ μeV and (b) $V_{\mathrm{ex}}=10$ μeV.

TABLE I. Numerical parameters.

Parameter	Symbol	Value
Electron effective mass	m_e	$0.043m_0$[a]
Hole effective mass	m_h	$0.450m_0$[a]
LO phonon energy	$\hbar\omega_{\mathrm{LO}}$	36.4 meV[a]
QD band gap	$\hbar\omega_0$	1.5 eV
Hole binding energy	$\Delta\varepsilon_v$	$1.5\hbar\omega_{\mathrm{LO}}$
Coulomb parameters	$V^{vc}=V^{vv}=V^{cc}$	25 μeV
	$V^{\mathrm{ex}}_{\uparrow\uparrow}=V^{\mathrm{ex}}_{\downarrow\downarrow}$	0 μeV
Photon lifetime in a cavity	κ	10 μeV
Electron-photon coupling	M	1 μeV
Radiative decay rate	Γ_{rad}	$(25\ \mathrm{ps})^{-1}$[b]

[a]Reference 54.
[b]Note that the radiative decay in a cavity is changed due to the Purcell effect.

tures, C will remain unaffected by the WL-induced dephasing Γ, since the scattering times are well above 1 ns, cf. Fig. 4. Starting at approximately 80 K, the WL starts to affect C as Γ reaches 1 ns^{-1}, which corresponds to an energy of 0.7 μeV, close to the optical coupling strength of $M=1$ μeV. The entanglement decreases for zero V_{ex} until it is entirely lost for temperatures beyond 100 K. For a higher FSS with $V_{\mathrm{ex}}\neq 0$, Fig. 9(c) shows that the degree of entanglement is lost slightly earlier around 80 K.

Finally, to pick up on the topic of temporal dynamics of the cascade addressed in Sec. IV A, let us consider a direct, single path leading to no entanglement. We will follow the blue HH (left) path in Fig. 5. The biexciton density $\langle\hat{B}^\dagger\hat{B}\rangle$ decays exponentially with two Γ (radiative and phonon-induced decay), giving rise to an intermediate coupled exciton-photon state $\langle\hat{X}_H^\dagger\hat{X}_H\hat{a}_H^\dagger\hat{a}_H\rangle$. Subsequently, when this state is sufficiently populated, it decays under emission of the exciton photon, and a two-photon density ρ_{HH} builds up. In the given range of parameters (see Table I in Appendix A), Fig. 10 shows that the decay cascade happens on a picosecond time scale. Even at low temperatures and $V_{\mathrm{ex}}=0$ μeV, due to a high-cavity loss κ (compared to the optical coupling strength M), both $\langle\hat{X}_H^\dagger\hat{X}_H\hat{a}_H^\dagger\hat{a}_H\rangle$ and ρ_{HH} are only weakly occupied. The inset in Fig. 10 is a logarithmic plot of the dynamics which clearly shows the different lifetimes of the involved quantities.

V. CONCLUSION

In summary, we present a microscopic theory of the reduced photon density matrix including all intermediate occurring states in a two-photon cascade emission. The interaction of the dot states with the WL via LO phonons gives rise to a strong reduction in the concurrence for temperatures above 100 K for typical InGaAs self-assembled QDs. This constitutes a severe restriction on room-temperature generation of entangled photons.

We further note, that the diagonal interaction of the QD states with longitudinal acoustical phonons is a major contribution to dephasing,[55,56] which will ultimately influence the quality of entanglement.[15] Regardless of their impact, we conclude that the inherit coupling to the WL imposes another fundamental limit to the high-temperature generation of polarization-entangled photons in quantum dot devices.

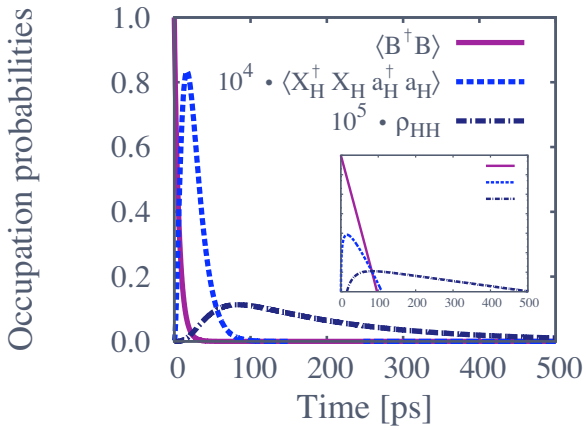

FIG. 10. (Color online) Dynamics of the cascade biexciton → exciton and one photon → ground state and two photons. Results for $V_{\mathrm{ex}}=0$ μeV at $T=0$ K. $\langle\hat{X}_H^\dagger\hat{X}_H\hat{a}_H^\dagger\hat{a}_H\rangle$ and ρ_{HH} are enlarged by a factor of 10^4 and 10^5, respectively. The inset shows the dynamics on a logarithmic scale.

ACKNOWLEDGMENTS

We would like to thank Stephen Hughes for helpful discussions. This work was financially supported by the Deutsche Forschungsgemeinschaft within the Sonderforschungsbereich 787 "Nanophotonik".

APPENDIX A: CARRIER-CARRIER INTERACTION AND EXCITON REPRESENTATION

Parts of the Hamiltonian in Eq. (5), accounting for the QD carriers and their interaction via the Coulomb potential $\hat{H}_{\mathrm{Coul}}=\hat{H}^{\mathrm{c}}_{\mathrm{QD},0}+\hat{H}^{\mathrm{c\text{-}c}}_{\mathrm{QD}}$, are conveniently rewritten as[14]

$$\hat{H}_{\mathrm{Coul}}=\sum_s\frac{\hbar\Omega_0}{2}(\hat{e}_s^\dagger\hat{e}_s-\hat{h}_s^\dagger\hat{h}_s)+\frac{1}{2}\sum_{ss'}(V^{ee}\hat{e}_s^\dagger\hat{e}_s\hat{e}_{s'}^\dagger\hat{e}_{s'}+V^{hh}\hat{h}_s^\dagger\hat{h}_s\hat{h}_{s'}^\dagger\hat{h}_{s'}+2V^{\mathrm{ex}}_{ss'}\hat{e}_s^\dagger\hat{h}_s^\dagger\hat{h}_{s'}\hat{e}_{s'}-2V^{he}\hat{e}_s^\dagger\hat{e}_s\hat{h}_{s'}^\dagger\hat{h}_{s'}). \tag{A1}$$

The corresponding Coulomb elements V^{ee}, V^{hh}, V^{he}, and $V^{\mathrm{ex}}_{ss'}$ mediate the interaction.

The explicit values of these matrix elements depend strongly on the geometry, size, and material of the QDs.[50,57–59] In this investigation, we focus on the impact of electron-LO phonon scattering on the concurrence. Therefore, we treat the matrix elements as parameters, which can be determined in experiments.[60]

The electron-photon matrix element leads to selection rules that have to be obeyed and so only electron-hole pairs with opposite spins couple. More important, the Pauli prin-

ciple forbids two carriers to be in the same state (that is, the spin state $s=|J,m_j\rangle$).

With these considerations, only four states remain to determine the system dynamics, defined by the following operators:

$$\hat{G}=\hat{h}_{\downarrow}\hat{h}_{\uparrow}\hat{h}_{\uparrow}^{\dagger}\hat{h}_{\downarrow}^{\dagger} \quad \text{ground-state operator}, \tag{A2}$$

$$\hat{B}=\hat{h}_{\uparrow}\hat{h}_{\downarrow}\hat{e}_{\uparrow}\hat{e}_{\downarrow} \quad \text{biexciton-state operator}, \tag{A3}$$

$$\hat{X}_{+}=\hat{h}_{\uparrow}\hat{h}_{\downarrow}\hat{h}_{\downarrow}^{\dagger}\hat{e}_{\downarrow} \quad \text{exciton-state operator 1}, \tag{A4}$$

$$\hat{X}_{-}=\hat{h}_{\downarrow}\hat{h}_{\uparrow}\hat{h}_{\uparrow}^{\dagger}\hat{e}_{\uparrow} \quad \text{exciton-state operator 2}. \tag{A5}$$

The exciton operators in Eqs. (A4) and (A5) emit into circular polarized light modes (σ_+ and σ_-), if the nondiagonal element $V_{\uparrow\downarrow}^{\mathrm{ex}}$ is zero. Commuting these operators with $\hat{H}_{\mathrm{Coul}}=\hat{H}_{\mathrm{QD},0}^{\mathrm{c}}+\hat{H}_{\mathrm{c\text{-}c}}^{\mathrm{c}}$, we find that they are eigenvectors of $\hat{H}_{\mathrm{Coul}}$. Their corresponding eigenvalues are $(\hbar\omega_G,\ \hbar\omega_H,\ \hbar\omega_V,\ \hbar\omega_B)$ with $\hbar\omega_G=0$, choosing zero as ground-state energy, and $\hbar\omega_B=4E_C+2\hbar\Omega_0+V_{\downarrow\downarrow}^{\mathrm{ex}}+V_{\uparrow\uparrow}^{\mathrm{ex}}$ with $E_C=\frac{1}{2}(V^{cc}+V^{vv}-2V^{vc})$. The exciton energies $\hbar\omega_H$ and $\hbar\omega_V$ are given in the two-particle basis as

$$\hbar\omega_{H/V}=\frac{1}{2}(2E_C+2\hbar\Omega_0+V_{\downarrow\downarrow}^{\mathrm{ex}}+V_{\uparrow\uparrow}^{\mathrm{ex}}\pm\delta). \tag{A6}$$

Responsible for the fine-structure splitting δ, compare Fig. 1, is the exchange splitting $V_{\uparrow\downarrow}^{\mathrm{ex}}$, which describes the repulsion and attraction forces induced by different spin conformations of electrons and holes. In the most general case, the exciton states could differ in energy due to contributions like $V_{\uparrow\uparrow}^{\mathrm{ex}}$ and $V_{\downarrow\downarrow}^{\mathrm{ex}}$. Given these elements, the most general fine-structure splitting can now be expressed quantitatively as $\delta:=\sqrt{(V_{\uparrow\uparrow}^{\mathrm{ex}}-V_{\downarrow\downarrow}^{\mathrm{ex}})^2+4|V_{\uparrow\downarrow}^{\mathrm{ex}}|^2}$. However, it is reasonable to assume that in semiconductor QDs no spin preferences exist, thus $V_{\uparrow\uparrow}^{\mathrm{ex}}-V_{\downarrow\downarrow}^{\mathrm{ex}}=0$, which leads to

$$\delta=2|V_{\uparrow\downarrow}^{\mathrm{ex}}|. \tag{A7}$$

To simplify the notation, we will refer to $V_{\uparrow\downarrow}^{\mathrm{ex}}$ as V_{ex}. In a reduced C_{2v} symmetry of strained dots, the off-diagonal element V^{ex} is nonzero and leads to a superposition of the exciton states

$$\hat{X}_H=\frac{1}{\sqrt{2}}(\hat{X}_{+}+\hat{X}_{-}),\quad \hat{X}_V=\frac{1}{\sqrt{2}}(\hat{X}_{+}-\hat{X}_{-}). \tag{A8}$$

Here, H and V refer to the linear polarization of the emitted photons in the biexciton cascade.

Using the space spanned by the new exciton operators, the Hamiltonian is rewritten as[59]

$$\hat{H}_{\mathrm{Coul}}=\hbar\omega_G\hat{G}^{\dagger}\hat{G}+\hbar\omega_H\hat{X}_H^{\dagger}\hat{X}_H+\hbar\omega_V\hat{X}_V^{\dagger}\hat{X}_V+\hbar\omega_B\hat{B}^{\dagger}\hat{B}$$

with $\hat{G}$ the ground state, $\hat{X}_{H/V}$ the exciton, and $\hat{B}$ the biexciton annihilation operator, corresponding to the excitonic level structure as depicted in Fig. 1(c).

APPENDIX B: QD ELECTRON-PHOTON INTERACTION

Commonly, the Hamiltonian of the electron-photon interaction is taken in rotating-wave approximation[31]

$$\hat{H}_{\mathrm{QD}}^{\mathrm{c\text{-}pt}}=\hbar M\sum_i(\hat{h}_{\uparrow}\hat{e}_{\downarrow}\hat{a}_{i\sigma_+}^{\dagger}+\hat{h}_{\downarrow}\hat{e}_{\uparrow}\hat{a}_{i\sigma_-}^{\dagger})+\mathrm{H.a.}, \tag{B1}$$

where the corresponding spin states couple to circular $\sigma_{\pm}$ polarized light, i is the mode of the emitted photon, and M denotes the electron-photon coupling matrix elements. Starting with Eq. (B1), we now switch to the new exciton operators $\hat{X}_{H/V}$ by inserting the unity relation of the electron-hole picture into Eq. (B1). After normal ordering and using the two-electron assumption, the electron-light interaction can be written as[50]

$$\hat{H}_{\mathrm{QD}}^{\mathrm{c\text{-}pt}}=\hbar M\sum_i(\hat{G}^{\dagger}\hat{X}_{+}+\hat{X}_{-}\hat{B})\hat{a}_{i\sigma_+}^{\dagger}+\hbar M\sum_i(\hat{G}^{\dagger}\hat{X}_{-}+\hat{X}_{+}\hat{B})\hat{a}_{i\sigma_-}^{\dagger}+\mathrm{H.a.} \tag{B2}$$

The electron-light interaction Hamiltonian $\hat{H}_{\mathrm{QD}}^{\mathrm{c\text{-}pt}}$ is transformed when the exciton operators are replaced with

$$\hat{X}_{+}=\frac{1}{\sqrt{2}}(\hat{X}_H+\hat{X}_V),\quad \hat{X}_{-}=\frac{1}{\sqrt{2}}(\hat{X}_H-\hat{X}_V). \tag{B3}$$

It is convenient to define new photon operators

$$\hat{a}_{iH}^{\dagger}=\frac{1}{\sqrt{2}}(\hat{a}_{i\sigma_+}^{\dagger}+\hat{a}_{i\sigma_-}^{\dagger}),$$

$$\hat{a}_{iV}^{\dagger}=\frac{1}{\sqrt{2}}(\hat{a}_{i\sigma_+}^{\dagger}-\hat{a}_{i\sigma_-}^{\dagger}). \tag{B4}$$

The Hamiltonian now takes the form

$$\hat{H}_{\mathrm{QD}}^{\mathrm{c\text{-}pt}}=\hbar M\sum_i(\hat{G}^{\dagger}\hat{X}_H\hat{a}_{iH}^{\dagger}+\hat{G}^{\dagger}\hat{X}_V\hat{a}_{iV}^{\dagger})+\hbar M\sum_i(\hat{X}_H^{\dagger}\hat{B}\hat{a}_{iH}^{\dagger}-\hat{X}_V^{\dagger}\hat{B}\hat{a}_{iV}^{\dagger})+\mathrm{H.a.} \tag{B5}$$

We assume that our QD is placed inside a nanocavity, which provides two different modes for the different polarizations H and V corresponding to different frequencies $\omega_H\neq\omega_V$.[28] Since only two modes exist within the cavity, we investigate a cavity-enhanced biexciton cascade. However, we remain in the weak-coupling regime since the cavity loss $\kappa=10\ \mu$eV is greater then the coupling strength to the field $M=1\ \mu$eV. Regarding only these two modes, the electron-light interaction Hamiltonian can be written in a compact form

$$\hat{H}_{\mathrm{QD}}^{\mathrm{c\text{-}pt}}=\hbar M(\hat{G}^{\dagger}\hat{X}_H\hat{a}_H^{\dagger}+\hat{G}^{\dagger}\hat{X}_V\hat{a}_V^{\dagger}+\hat{X}_H^{\dagger}\hat{B}\hat{a}_H^{\dagger}-\hat{X}_V^{\dagger}\hat{B}\hat{a}_V^{\dagger})+\mathrm{H.a.} \tag{B6}$$

At this point, the total Hamiltonian is written with the new exciton and photon operators (H, V).

APPENDIX C: EQUATIONS OF MOTION

The temporal evolution of the driving terms in Eq. (14) is given by

$$\partial_t\langle \hat{G}^\dagger \hat{X}_H \hat{a}_V^\dagger \hat{a}_V^\dagger \hat{a}_H\rangle = i(-\omega_H + 2\omega_V^{\mathrm{cav}} - \omega_H^{\mathrm{cav}} + i\Gamma/2 + 3i\kappa) \times \langle \hat{G}^\dagger \hat{X}_H \hat{a}_V^\dagger \hat{a}_V^\dagger \hat{a}_H\rangle - 2iM\langle \hat{X}_V^\dagger \hat{X}_H \hat{a}_V^\dagger \hat{a}_H\rangle + iM\langle \hat{G}^\dagger \hat{B} \hat{a}_V^\dagger \hat{a}_V^\dagger\rangle \quad \text{(C1)}$$

and

$$\partial_t\langle \hat{X}_V^\dagger \hat{G} \hat{a}_V^\dagger \hat{a}_H \hat{a}_H\rangle = i(\omega_V + \omega_V^{\mathrm{cav}} - 2\omega_H^{\mathrm{cav}} + i\Gamma/2 + 3i\kappa) \times \langle \hat{X}_V^\dagger \hat{G} \hat{a}_V^\dagger \hat{a}_H \hat{a}_H\rangle + 2iM\langle \hat{X}_V^\dagger \hat{X}_H \hat{a}_V^\dagger \hat{a}_H\rangle + iM\langle \hat{B}^\dagger \hat{G} \hat{a}_H \hat{a}_H\rangle. \quad \text{(C2)}$$

The driving terms of the two-photon density matrix, in turn, couple to combined exciton and photon coherences $\hat{X}_V^\dagger \hat{X}_H \hat{a}_V^\dagger \hat{a}_H$ and to the direct decay channel from $|B\rangle$ to $|G\rangle$ emitting two photons with the same polarization, $\hat{G}^\dagger \hat{B} \hat{a}_V^\dagger \hat{a}_V^\dagger$, see orange box in Fig. 5. Crucial for entangling the two decay paths is the exciton coherence, assisted by a photon coherence, see red box in Fig. 5

$$\partial_t\langle \hat{X}_V^\dagger \hat{X}_H \hat{a}_V^\dagger \hat{a}_H\rangle = i(\omega_V - \omega_H + \omega_V^{\mathrm{cav}} - \omega_H^{\mathrm{cav}} + i\Gamma + 2i\kappa) \times \langle \hat{X}_V^\dagger \hat{X}_H \hat{a}_V^\dagger \hat{a}_H\rangle - iM\langle \hat{G}^\dagger \hat{X}_H \hat{a}_V^\dagger \hat{a}_V^\dagger \hat{a}_H\rangle + iM\langle \hat{B}^\dagger \hat{X}_H \hat{a}_H\rangle + iM\langle \hat{X}_V^\dagger \hat{G} \hat{a}_V^\dagger \hat{a}_H \hat{a}_H\rangle + iM\langle \hat{X}_V^\dagger \hat{B} \hat{a}_V^\dagger\rangle. \quad \text{(C3)}$$

In this equation, the two paths interfere. The influence in the two-particle correlation $\langle \hat{X}_V^\dagger \hat{X}_H \hat{a}_V^\dagger \hat{a}_H\rangle$ increases the degree of entanglement as this term couples back to the driving terms of ρ_{VH}, Eqs. (C1) and (C2). Here, the resonance condition of the frequencies is essential ($\omega_V - \omega_H = \omega_V^{\mathrm{cav}} - \omega_H^{\mathrm{cav}} = \delta$). A high detuning δ will diminish the contribution of Eq. (C3) to the cascade, and both paths cannot interfere.

The other characteristic and important quantities in the two-electron biexciton-cascade situation [cf. with two coupled QDs (Ref. 50)] are the two-photon polarizations

$$\partial_t\langle \hat{G}^\dagger \hat{B} \hat{a}_V^\dagger \hat{a}_V^\dagger\rangle = i(-\omega_B + 2\omega_V^{\mathrm{cav}} + i\Gamma + 2i\kappa)\langle \hat{G}^\dagger \hat{B} \hat{a}_V^\dagger \hat{a}_V^\dagger\rangle + iM\langle \hat{G}^\dagger \hat{X}_H \hat{a}_V^\dagger \hat{a}_V^\dagger \hat{a}_H\rangle - iM\langle \hat{G}^\dagger \hat{X}_V \hat{a}_V^\dagger \hat{a}_V^\dagger \hat{a}_V\rangle - 2iM\langle \hat{X}_V^\dagger \hat{B} \hat{a}_V^\dagger\rangle \quad \text{(C4)}$$

and

$$\partial_t\langle \hat{B}^\dagger \hat{G} \hat{a}_H \hat{a}_H\rangle = i(\omega_B - 2\omega_H^{\mathrm{cav}} + i\Gamma + 2i\kappa)\langle \hat{B}^\dagger \hat{G} \hat{a}_H \hat{a}_H\rangle, \quad \text{(C5)}$$

$$-iM\langle \hat{X}_H^\dagger \hat{G} \hat{a}_H^\dagger \hat{a}_H \hat{a}_H\rangle + iM\langle \hat{X}_V^\dagger \hat{G} \hat{a}_V^\dagger \hat{a}_H \hat{a}_H\rangle + 2iM\langle \hat{B}^\dagger \hat{X}_H \hat{a}_H\rangle. \quad \text{(C6)}$$

Each path in the cascade has one biexciton-to-ground-state transition like $\hat{G}^\dagger \hat{B} \hat{a}_V^\dagger \hat{a}_V^\dagger$. Its dynamics couples the biexciton-to-exciton transition $\hat{X}_V^\dagger \hat{B} \hat{a}_V^\dagger$ with both exciton-to-ground-state transitions $\hat{G}^\dagger \hat{X}_i$. Remarkably, the origin of the entanglement is directly visible, since a quantity of a different path enters in Eq. (C4): $\langle \hat{G}^\dagger \hat{X}_H \hat{a}_V^\dagger \hat{a}_V^\dagger \hat{a}_H\rangle$. Here again, the two paths interfere. For maximal entanglement, the contributions of the different paths $\hat{G}^\dagger \hat{X}_H$ and $\hat{G}^\dagger \hat{X}_V$ to the expectation values should be equally weighted. The photon-assisted biexciton-to-exciton transition enters in the two-photon polarization and drives this quantity via the biexciton decay

$$\partial_t\langle \hat{B}^\dagger \hat{X}_H \hat{a}_H\rangle = i(\omega_B - \omega_H - \omega_H^{\mathrm{cav}} + 3i\Gamma/2 + i\kappa)\langle \hat{B}^\dagger \hat{X}_H \hat{a}_H\rangle - iM\langle \hat{X}_H^\dagger \hat{X}_H \hat{a}_H^\dagger \hat{a}_H\rangle + iM\langle \hat{X}_V^\dagger \hat{X}_H \hat{a}_V^\dagger \hat{a}_H\rangle + iM\langle \hat{B}^\dagger \hat{B}\rangle + iM\langle \hat{B}^\dagger \hat{G} \hat{a}_H \hat{a}_H\rangle, \quad \text{(C7)}$$

$$\partial_t\langle \hat{X}_V^\dagger \hat{B} \hat{a}_V^\dagger\rangle = i(-\omega_B + \omega_V + \omega_V^{\mathrm{cav}} + 3i\Gamma/2 + i\kappa)\langle \hat{X}_V^\dagger \hat{B} \hat{a}_V^\dagger\rangle - iM\langle \hat{G}^\dagger \hat{B} \hat{a}_V^\dagger \hat{a}_V^\dagger\rangle + iM\langle \hat{B}^\dagger \hat{B}\rangle + iM\langle \hat{X}_V^\dagger \hat{X}_H \hat{a}_V^\dagger \hat{a}_H\rangle - iM\langle \hat{X}_V^\dagger \hat{X}_V \hat{a}_V^\dagger \hat{a}_V\rangle. \quad \text{(C8)}$$

The occurring biexciton as well as the intermediate exciton-photon densities are driven by the biexciton-exciton transition $\langle \hat{X}_i^\dagger \hat{B} \hat{a}_i^\dagger\rangle$

$$\partial_t\langle \hat{X}_H^\dagger \hat{X}_H \hat{a}_H^\dagger \hat{a}_H\rangle = -(\Gamma + 2\kappa)\langle \hat{X}_H^\dagger \hat{X}_H \hat{a}_H^\dagger \hat{a}_H\rangle - 2\,\mathrm{Im}(M\langle \hat{X}_H^\dagger \hat{B} \hat{a}_H^\dagger\rangle + M\langle \hat{X}_H^\dagger \hat{G} \hat{a}_H^\dagger \hat{a}_H \hat{a}_H\rangle), \quad \text{(C9)}$$

$$\partial_t\langle \hat{X}_V^\dagger \hat{X}_V^\dagger \hat{a}_V^\dagger \hat{a}_V\rangle = -(\Gamma + 2\kappa)\langle \hat{X}_V^\dagger \hat{X}_V^\dagger \hat{a}_V^\dagger \hat{a}_V\rangle + 2\,\mathrm{Im}(M\langle \hat{X}_V^\dagger \hat{B} \hat{a}_V^\dagger\rangle - M\langle \hat{X}_V^\dagger \hat{G} \hat{a}_V^\dagger \hat{a}_V \hat{a}_V\rangle). \quad \text{(C10)}$$

From the perspective of the cascade, our course of action so far put the cart before the horse since the actual dynamics start with a loaded biexciton density $\langle \hat{B}^\dagger \hat{B}\rangle$. In the visualization of the complex interplay, Fig. 5, we followed a bottom-to-top trail through the cascade, starting with the concurrence determining ρ_{VH}. The biexciton $\langle \hat{B}^\dagger \hat{B}\rangle$ as the top element of the scheme decays via the H or the V intermediate exciton-to-ground-state path

$$\partial_t\langle \hat{B}^\dagger \hat{B}\rangle = -2\Gamma\langle \hat{B}^\dagger \hat{B}\rangle + 2\,\mathrm{Im}(M\langle \hat{X}_H^\dagger \hat{B} \hat{a}_H^\dagger\rangle - M\langle \hat{X}_V^\dagger \hat{B} \hat{a}_V^\dagger\rangle). \quad \text{(C11)}$$

To complete the set of equations, two higher-order photon-assisted exciton-to-ground-state transitions of the direct and thus not entangled path are necessary

$$\partial_t\langle \hat{G}^\dagger \hat{X}_H \hat{a}_H^\dagger \hat{a}_H^\dagger \hat{a}_H\rangle = i(-\omega_H + \omega_H^{\mathrm{cav}} + i\Gamma/2 + 3i\kappa) \times \langle \hat{G}^\dagger \hat{X}_H \hat{a}_H^\dagger \hat{a}_H^\dagger \hat{a}_H\rangle - 2iM\langle \hat{X}_H^\dagger \hat{X}_H \hat{a}_H^\dagger \hat{a}_H\rangle + iM\langle \hat{G}^\dagger \hat{B} \hat{a}_H^\dagger \hat{a}_H^\dagger\rangle, \quad \text{(C12)}$$

$$\partial_t\langle \hat{G}^\dagger \hat{X}_V \hat{a}_V^\dagger \hat{a}_V^\dagger \hat{a}_V\rangle = i(-\omega_V + \omega_V^{\mathrm{cav}} + i\Gamma/2 + 3i\kappa)\langle \hat{G}^\dagger \hat{X}_V \hat{a}_V^\dagger \hat{a}_V^\dagger \hat{a}_V\rangle - 2iM\langle \hat{X}_V^\dagger \hat{X}_V \hat{a}_V^\dagger \hat{a}_V\rangle - iM\langle \hat{G}^\dagger \hat{B} \hat{a}_V^\dagger \hat{a}_V^\dagger\rangle. \quad \text{(C13)}$$

With these polarization Eqs. (C12) and (C13), the diagonal elements $i=H$ and V of the density matrix of the polarization subspace are given

$$\partial_t\langle \hat{a}_i^\dagger \hat{a}_i^\dagger \hat{a}_i \hat{a}_i\rangle = -4\kappa\langle \hat{a}_i^\dagger \hat{a}_i^\dagger \hat{a}_i \hat{a}_i\rangle - 4\,\mathrm{Im}(M\langle \hat{G}^\dagger \hat{X}_i^\dagger \hat{a}_i^\dagger \hat{a}_i^\dagger \hat{a}_i\rangle). \tag{C14}$$

*alex@itp.physik.tu-berlin.de

[1] T. B. Pittman, B. C. Jacobs, and J. D. Franson, Phys. Rev. A **66**, 042303 (2002).
[2] D. Stucki, N. Gisin, O. Guinnard, G. Ribordy, and H. Zbinden, New J. Phys. **4**, 41 (2002).
[3] N. Gisin, G. Ribordy, W. Tittel, and H. Zbinden, Rev. Mod. Phys. **74**, 145 (2002).
[4] A. Poppe, A. Fedrizzi, R. Ursin, H. Bohm, T. Lorunser, O. Maurhardt, M. Peev, M. Suda, C. Kurtsiefer, H. Weinfurter, T. Jennewein, and A. Zeilinger, Opt. Express **12**, 3865 (2004).
[5] D. Bouwmeester, J. Pan, K. Mattle, M. Eibl, H. Weinfurter, and A. Zeilinger, Nature (London) **390**, 575 (1997).
[6] C. H. Bennett, G. Brassard, C. Crépeau, R. Jozsa, A. Peres, and W. K. Wootters, Phys. Rev. Lett. **70**, 1895 (1993).
[7] J. Brendel, N. Gisin, W. Tittel, and H. Zbinden, Phys. Rev. Lett. **82**, 2594 (1999).
[8] K. Edamatsu, G. Oohata, R. Shimizu, and T. Itoh, Nature (London) **431**, 167 (2004).
[9] S. Fasel, O. Alibart, S. Tanzilli, P. Baldi, A. Beveratos, N. Gisin, and H. Zbinden, New J. Phys. **6**, 163 (2004).
[10] Z. Y. Ou and L. Mandel, Phys. Rev. Lett. **61**, 50 (1988).
[11] Y. H. Shih and C. O. Alley, Phys. Rev. Lett. **61**, 2921 (1988).
[12] O. Benson, C. Santori, M. Pelton, and Y. Yamamoto, Phys. Rev. Lett. **84**, 2513 (2000).
[13] A. Schliwa, M. Winkelnkemper, A. Lochmann, E. Stock, and D. Bimberg, Phys. Rev. B **80**, 161307(R) (2009).
[14] V. M. Axt, T. Kuhn, A. Vagov, and F. M. Peeters, Phys. Rev. B **72**, 125309 (2005).
[15] U. Hohenester, G. Pfanner, and M. Seliger, Phys. Rev. Lett. **99**, 047402 (2007).
[16] D. Bimberg, M. Grundmann, and N. N. Ledentsov, *Quantum Dot Heterostructures* (Wiley, Chichester, 1999).
[17] T. Inoshita and H. Sakaki, Phys. Rev. B **46**, 7260 (1992).
[18] D. Bimberg, E. Stock, A. Lochmann, A. Schliwa, J. Tofflinger, W. Unrau, M. Munnix, S. Rodt, V. Haisler, A. Toropov, A. Bakarov, and A. Kalagin, IEEE Photonics J. **1**, 58 (2009).
[19] J. Wolters, M.-R. Dachner, E. Malić, M. Richter, U. Woggon, and A. Knorr, Phys. Rev. B **80**, 245401 (2009).
[20] Z. Yuan, B. E. Kardynal, R. M. Stevenson, A. J. Shields, C. J. Lob, K. Cooper, N. S. Beattie, D. A. Ritchie, and M. Pepper, Science **295**, 102 (2002).
[21] O. Stier, M. Grundmann, and D. Bimberg, Phys. Rev. B **59**, 5688 (1999).
[22] P. Y. Yu and M. Cardona, *Fundamentals of Semiconductors* (Springer, New York, 2005).
[23] A. L. Efros, M. Rosen, M. Kuno, M. Nirmal, D. J. Norris, and M. Bawendi, Phys. Rev. B **54**, 4843 (1996).
[24] C. Weisbuch and B. Winter, *Quantum Semiconductor Structures* (Academic Press, San Diego, 1991).
[25] G. D. Scholes, J. Chem. Phys. **121**, 10104 (2004).
[26] A. Lochmann, E. Stock, J. Töfflinger, W. Unrau, A. Toropov, A. Bakarov, V. Haisler, and D. Bimberg, Electron. Lett. **45**, 566 (2009).
[27] K. Edamatsu, Jpn. J. Appl. Phys. **46**, 7175 (2007).
[28] K. Hennessy, C. Högerle, E. Hu, A. Badolato, and A. Imamoğlu, Appl. Phys. Lett. **89**, 041118 (2006).
[29] R. M. Stevenson, R. Young, P. Atkinson, K. Cooper, D. Ritchie, and A. Shields, Nature (London) **439**, 179 (2006).
[30] D. F. V. James, P. G. Kwiat, W. J. Munro, and A. G. White, Phys. Rev. A **64**, 052312 (2001).
[31] L. Mandel and E. Wolf, *Optical Coherence and Quantum Optics* (Cambridge University Press, Cambridge, 1995).
[32] F. Troiani, J. I. Perea, and C. Tejedor, Phys. Rev. B **74**, 235310 (2006).
[33] M. Benyoucef, S. M. Ulrich, P. Michler, J. Wiersig, F. Jahnke, and A. Forchel, New J. Phys. **6**, 91 (2004).
[34] W. K. Wootters, Phys. Rev. Lett. **80**, 2245 (1998).
[35] V. Coffman, J. Kundu, and W. K. Wootters, Phys. Rev. A **61**, 052306 (2000).
[36] M. Vachon, S. Raymond, A. Babinski, J. Lapointe, Z. Wasilewski, and M. Potemski, Phys. Rev. B **79**, 165427 (2009).
[37] I. Magnusdottir, A. V. Uskov, S. Bischoff, B. Tromborg, and J. Mørk, J. Appl. Phys. **92**, 5982 (2002).
[38] E. A. Muljarov and R. Zimmermann, Phys. Rev. Lett. **98**, 187401 (2007).
[39] E. A. Muljarov and R. Zimmermann, Phys. Status Solidi B **245**, 1106 (2008).
[40] J. Seebeck, T. R. Nielsen, P. Gartner, and F. Jahnke, Phys. Rev. B **71**, 125327 (2005).
[41] P. Machnikowski, Phys. Rev. B **78**, 195320 (2008).
[42] B. Krummheuer, V. M. Axt, T. Kuhn, I. D'Amico, and F. Rossi, Phys. Rev. B **71**, 235329 (2005).
[43] F. H. M. Faisal, *Theory of Multiphoton Processes* (Plenum Press, London, 1987).
[44] G. D. Mahan, *Many-Particle Physics* (Plenum Press, New York, 1990).
[45] M.-R. Dachner, E. Malic, M. Richter, A. Carmele, J. Kabuss, A. Wilms, J.-E. Kim, G. Hartmann, J. Wolters, U. Bandelow, and A. Knorr, Phys. Status Solidi B **247**(4), 809 (2010).
[46] We note that in Ref. 45 we provided only the effective coupling elements in the low-density limit, which do not contain the Pauli-blocking contributions due to WL occupations.
[47] I. Waldmüller, J. Förstner, S.-C. Lee, A. Knorr, M. Woerner, K. Reimann, R. A. Kaindl, T. Elsaesser, R. Hey, and K. H. Ploog, Phys. Rev. B **69**, 205307 (2004); T. Shih, K. Reimann, M. Woerner, T. Elsaesser, I. Waldmüller, A. Knorr, R. Hey, and K. H. Ploog, *ibid.* **72**, 195338 (2005).
[48] M.-R. Dachner, J. Wolters, A. Knorr, and M. Richter, Conference on Lasers and Electro-Optics/International Quantum Electronics Conference (Optical Society of America, Washington D.C., 2009) p. JWA119.
[49] M. O. Scully and M. S. Zubairy, *Quantum Optics* (Cambridge University Press, Cambridge, 1997).
[50] A. Carmele, A. Knorr, and M. Richter, Phys. Rev. B **79**, 035316

(2009).
[51] G. A. Narvaez, G. Bester, A. Franceschetti, and A. Zunger, Phys. Rev. B **74**, 205422 (2006).
[52] H. Carmichael, *Statistical Methods in Quantum Optics 1; Master Equation and Fokker-Planck Equations* (Springer, New York, 1999).
[53] This value depends on the light coupling strength and the radiative dephasing.
[54] *Semiconductors: Group IV Elements, IV-IV and III-V Compounds*, Landolt-Börnstein, Group III Condensed Matter Vol. III/41b, edited by U. Rössler (Springer, New York, 2002).
[55] P. Borri, W. Langbein, S. Schneider, U. Woggon, R. L. Sellin, D. Ouyang, and D. Bimberg, Phys. Rev. Lett. **87**, 157401 (2001).
[56] F. Milde, A. Knorr, and S. Hughes, Phys. Rev. B **78**, 035330 (2008).
[57] T. Takagahara, Phys. Rev. B **62**, 16840 (2000).
[58] T. Takagahara, Phys. Rev. B **47**, 4569 (1993).
[59] M. Richter, K. J. Ahn, A. Knorr, A. Schliwa, D. Bimberg, M. E.-A. Madjet, and T. Renger, Phys. Status Solidi B **243**, 2302 (2006).
[60] W. Langbein, P. Borri, U. Woggon, V. Stavarache, D. Reuter, and A. D. Wieck, Phys. Rev. B **69**, 161301(R) (2004).